Water Resources Research

RESEARCH ARTICLE
10.1029/2018WR023639

Meandering Evolution and Width Variations: A Physics-Statistics-Based Modeling Approach

Sergio Lopez Dubon[1] **and Stefano Lanzoni**[1]

[1]Department of Civil, Environmental and Architectural Engineering, University of Padua, Padua, Italy

Key Points:
- Statistics of channel width variations in alluvial rivers can be described trough a Generalized Extreme Value (GEV) probability density function
- Modeling of channel width evolution constrained by statistics provides a river-specific characterization of width fluctuations that can be coupled with planform evolution models
- Long-term simulations of planform channel evolution accounting for width variations reveal the presence of looping cycles that resemble closely the observed river behavior

Supporting Information:
- Supporting Information S1

Correspondence to:
S. Lopez Dubon,
stefano.lanzoni@unipd.it

Citation:
Lopez Dubon S., & Lanzoni, S. (2019). Meandering evolution and width variations: A physics-statistics-based modeling approach. *Water Resources Research*, *55*. https://doi.org/10.1029/2018WR023639

Received 6 JUL 2018
Accepted 13 NOV 2018
Accepted article online 26 NOV 2018

Abstract Many models have been so far proposed to simulate and understand the long-term evolution of meandering rivers. Nevertheless, some modeling problems still need to be solved, for example, the physical soundness of long-term simulations when width variations are accounted for. The present work proposes the use of statistical tools to capture the spatiotemporal variations of channel width and to embed their effect into a physics-statistics-based model that simulates the river bank evolution. Erosion and deposition processes are assumed to act independently, with a specific shear stress threshold for each of them. In addition, the width evolution is linked with a river-specific probability density function. The analysis of a representative sample of meandering configurations, extracted from Landsat images, indicates that in many cases a generalized extreme value distribution nicely describes the along-channel distribution of cross-section width. For a given river, the parameters of this distribution keep almost constant in time. Significant variations are observed only after cutoff events that shorten the length of the river. The constraint of the river width based on the assumption of a generalized extreme value distribution ensures physically plausible configurations as the river moves throughout the floodplain, adapting continuously its local width. The application of the model to a reach of the Ucayali River appears to reasonably reproduce the planform river morphodynamics and yields realistic values of the cross-section widths.

1. Introduction

A meander consists of a series of two alternate bends, connected at the points of inflection by short, almost straight crossings. The presence of single thread meandering rivers exhibiting a continuous sequence of such bends is widespread in alluvial floodplains (Hooke, 2013; Howard, 1992). The study of meanders has thus fascinated the scientific community, which, since a long time, has tried not only to quantify the complexity of their planforms but also to model their morphodynamic evolution (Camporeale et al., 2005; Frascati & Lanzoni, 2010; Güneralp et al., 2012; Hooke, 2007; Howard & Hemberger, 1991).

Many theories have been proposed to understand the development of meanders. One of the most popular considers meanders as a dynamic system that migrates and evolves along a floodplain as a consequence of the complex interactions involving the channel planform, the in-channel flow, and sediment transport. The mechanism leading to the formation of meanders is known as bend instability (Blondeaux & Seminara, 1985; Ikeda et al., 1981). Indeed, a perturbation of an initially straight channel alignment grows, driven by bank erosion, and eventually leads to the development of a meandering pattern (Seminara, 2006). Specifically, channel lateral migration is driven by the difference of flow velocity between the outer and inner bank (excess bank velocity ΔU), which, in turn, is strongly affected by the secondary flow circulations induced by channel axis curvature, bed topography, and width variations (Bolla Pittaluga & Seminara, 2011; Zolezzi et al., 2012).

A number of models with a different degree of approximation have been so far developed for simulating the evolution of meandering rivers (Camporeale et al., 2007). Generally, the relevant conservation equations for the in-channel flow are averaged over the depth and the effects of secondary circulations are suitably parametrized (quasi-2-D models) taking advantage of linearization (Frascati & Lanzoni, 2013; Zolezzi & Seminara, 2001). The resulting models have in general a reasonable accuracy, provided some dimensionless parameters keep small (see, e.g., Bolla Pittaluga & Seminara, 2011). In addition, their low computational coast makes them ideal for long-term simulations (Frascati & Lanzoni, 2010).

Also, the river bank movement (driven by erosion/accretion processes) is usually described in a very simplified manner, relating linearly the rate of channel axis migration ξ to the excess bank velocity through a

dimensionless erosion coefficient E (Ikeda et al., 1981):

$$\xi = E\Delta U \tag{1}$$

The value of E depends on the bank strength and is usually calibrated using field data (Constantine et al., 2009). Even if this formulation seems to mimic reasonably the behavior of natural meanders (Bogoni et al., 2017; Frascati & Lanzoni, 2009), it is very simplified. In particular, the eroding outer bank is assumed to be destroyed at a rate dictated by the flow, while the depositing inner bank migrates passively in response and, consequently, a constant bankfull channel width is maintained.

Nevertheless, the presence of spatial width variations is typical of many rivers. These variations are the results of both allogenic bank-driven mechanisms and of in-channel autogenic hydromorphodynamic processes (Zolezzi et al., 2012). Allogenic width fluctuations are related to the difference in lateral rate of migration displayed by the outer and inner banks of a bend. A faster retreat of the outer bank implies a channel widening (bank pull), while a faster accretion of the inner point bar determines a channel narrowing (bar push; Parker et al., 2011) . On the other hand, nonlinear curvature-width interactions of the in-channel flow are responsible for the growth of midchannel bars, which, in turn, promote width oscillations and ultimately affect the bend instability mechanism.

Recently, many researchers (e.g., Asahi et al., 2013; Chen & Duan, 2006; Darby et al., 2002; Darby & Delbono, 2002; Eke, Czapiga, et al., 2014; Eke, Parker, & Shimizu, 2014; Motta et al., 2012; Nagata et al., 2000; Parker et al., 2011) tried to account for channel width variations, introducing more refined treatments of the lateral bank movements. In particular, Parker et al. (2011) proposed a model in which the migration of the eroding outer bank and of the depositing inner bank is treated separately. The erosion rate, depending on the noncohesive bank material, is moderated by the cohesive slump blocks produced cyclically by bank collapse events and subsequently eroded by the river flow. The accretion of the inner point bar is assumed to be controlled by the sediment captured by the encroaching vegetation. In the long term, the model simulates a river width that fluctuates around a mean value, depending on the continuous interplay between bank-pull and bar-push mechanisms. This treatment of bank narrowing/widening has been coupled to a fully nonlinear depth-averaged morphodynamics model by Eke, Czapiga, et al. (2014) to study the coevolution over time of local channel curvature, width, and streamwise slope. The simulations appear to qualitatively reproduce the broad range of river width-curvature correlations observed in nature, as a function of the ratio between the reference values of bank erosion and bank deposition rates. Nevertheless, no systematic simulations have been carried out with such model in the long term, and a thorough comparison between numerical results and field evidence is still missing.

The aim of the present study is twofold. The first is to evaluate the statistical properties of the spatiotemporal distributions of channel width distributions observed in an extensive set of alluvial rivers, selected all around the world. The second is to embed this statistical characterization in a physics-statistics-based model for the river bank movements. We anticipate that the along-river distribution of cross-section width in many cases is nicely represented by a general extreme value (GEV) probability density function (PDF). The form of the GEV (described by three parameters) is observed to vary in time after strong modifications of the river path, for example, consequent to cutoff processes. However, after any significant morphological change, the GEV tends to progressively recover its preevent form. It is thus deemed that, in the absence of important changes in the hydrological and/or sedimentological regimes, a given river can be characterized by a specific GEV. Based on this assumption, we develop a model whereby allogenic width variations, generated by the interplay of bank erosion and accretion process, are constrained within a meaningful range of values through the GEV distribution. The application of the model to simulate the evolution of the Ucayali River confirms that the proposed approach allows stable middle- and long-term simulations with realistic values of channel width variations.

2. Material and Methods

The first step of this study consists of the creation of an extensive data set of channel cross-section widths extracted from Landsat images. These data are analyzed statistically to infer the possible existence of specific trends in width distributions and in the corresponding moments. The results of these analyses are then embedded in a mathematical model that simulates the planform evolution of meandering rivers.

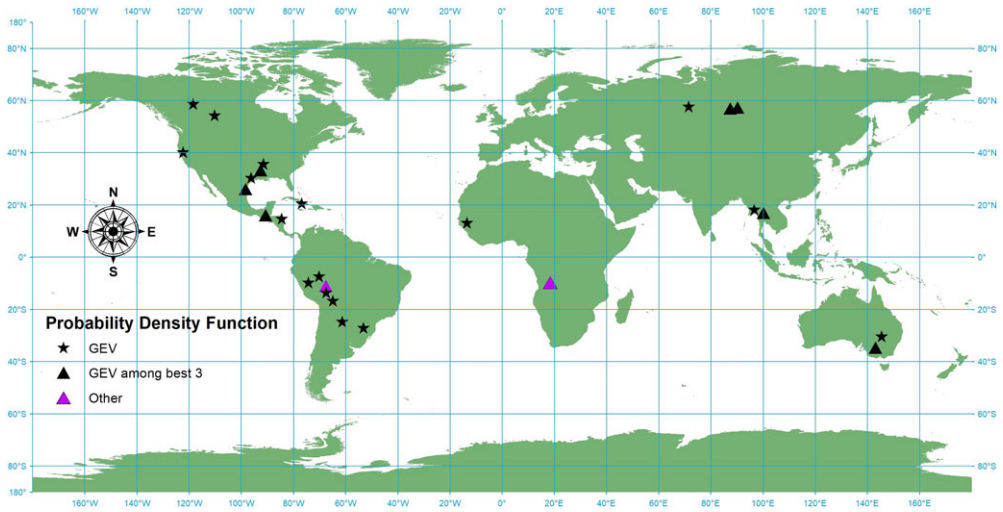

Figure 1. Location on the world map of the 26 investigated rivers. The stars indicate rivers in which a GEV distribution provides the best or the second best fitting PDF of along-channel widths. Black triangles denote rivers in which the GEV is among the best three fitting PDFs. The rivers coordinates are those in Table S1 in the supporting information. GEV = generalized extreme value; PDF = probability density function.

2.1. Remote Sensing Data

Obtaining detailed topographic field data can, in general, be an expensive and time-consuming task, in particular, when large spatial and temporal scales need to be considered. In the case of meandering rivers the increasing availability of satellite images ensures the possibility to build up an extensive and reliable data set from which river planform configurations and channel width distributions can be extracted. In this contribution we used Landsat images provided by the U.S. Geological Survey Earth Explorer portal (https://earthexplorer.usgs.gov/), which have the advantage of being free, georeferenced, and available since 1972 (U.S. Geological Survey, 2015). Each image corresponds to a single temporal instant and, differently from other free sources of satellite images, covers the entire extension of a given river. Most of the images used in this study were taken from Landsat 8 Operational Land Imager and Thermal Infrared Sensor.

The selected images include a large sample of alluvial rivers, selected all around the world, from tropical to high latitudes, to account for different hydrological regimes, type of soils, and land uses (Figure 1). In general, the more recent and the oldest available images were selected for each river, considering those with bankfull or nearly bankfull conditions and, anyway, disregarding those with high cloud cover levels. In the case of the Chixoy, Bermejo, Sacramento, Segovia, and Ucayali Rivers the images collected in different, possibly consecutive years have been also considered. In the selection of the images, particular attention has been paid to monitor the river before and after important changes of its planimetric configuration, determined by natural cutoff events or human interventions.

A case of particular interest considered here is that of the Ucayali River, which is characterized by a high rate of migration, up to 750 m/year (Constantine et al., 2014; Schwenk et al., 2015; Wickert et al., 2013). The drainage basin has an approximated area of 3.5×10^5 km^2, is located in Perú, and drains part of the upper Amazon basin until it joins with the Marañon river, forming the Amazon River. The mean annual discharge is about 6,905 m^3/s at Lagarto gauging station, where the area of the drainage basin is 1.9×10^5 km^2. The discharge increases up to 8,675 m^3/s at Pucallpa gauging station, draining an area of 2.6×10^5 km^2 (Santini et al., 2014; SENAMHI, 2016). The mean slope of the overall reach is 4.9×10^{-5} m/m, while the slope between Pucallpa and Tiruntan reduces to 3.3×10^{-5} m/m. The mean sediment size d_{50} varies from 0.25 to 0.4 mm and, hence, is transported mainly in suspension, with concentration ranging from 1,260 mg/L at Lagarto to 950 mg/L at Pucallpa (Santini et al., 2014). The level of human interventions is quite low. No significant hydraulic structures exist that interfere with the natural evolution of the river (Ettmer & Alvarado-Ancieta, 2010), even if a chute cutoff has been artificially induced in 1997 (Abizaid, 2005). Detailed geometrical information about the river course is available from RIVMAP (Schwenk et al., 2017).

For each Landsat image, the river axis planform and the corresponding along-channel distribution of cross-section width have been extracted as follows. First, the areas characterized by the presence of water

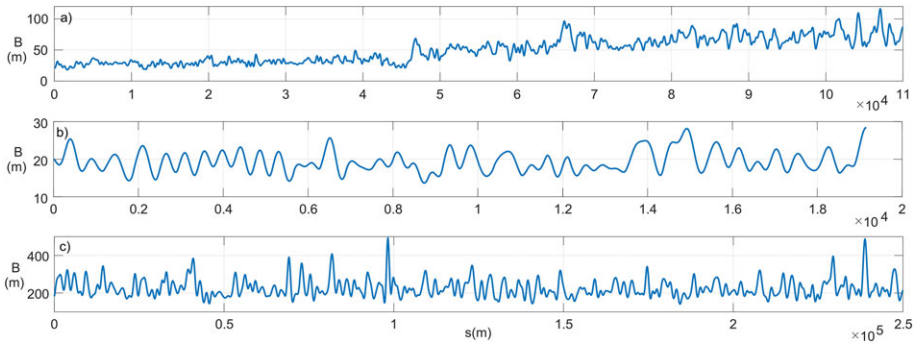

Figure 2. Examples of the along-channel distributions of the channel half-width $B(s)$ computed for the (a) Cauto, (b) Beaver, and (c) Beni Rivers. The s coordinate coincides with the channel axis and is directed downstream.

were classified by employing the Normalized Difference Water Index (NDWI) and its modified version (MNDWI), defined from multiband satellite images as (McFeeters, 1996; Xu, 2006)

$$\text{NDWI} = \frac{\text{G-NIR}}{\text{G+NIR}}, \qquad \text{MNDWI} = \frac{\text{G-SWIR1}}{\text{G+SWIR1}}, \tag{2}$$

where G is a free green band, NIR is a near-infrared band, and SWIR1 is a shortwave infrared band. These indexes enhance open water features and suppress or even remove vegetation and soil noise, as well as built-up land noise. They typically range in the interval $[-1, +1]$, and positive values are typically taken to indicate open water areas. Next, the river banks were delimited manually by using the software ArcMap, removing the imperfections arising from the automatic classification made on the basis of NDWI and MNDWI indexes. Finally, the central river axis was extracted as the line equidistant from the two river banks.

The coordinates of the points composing the bank and the central axis lines are expressed in the projected system Universal Transverse Mercator/World Geodetic System 1984, in order to work directly with actual distances. The half-width $B(s)$ of the channel cross section is computed as the distance of the channel axis from each bank and is referred to the curvilinear coordinate s coinciding with the channel axis and directed downstream (see, e.g., Figure 2).

Even though the Landsat images were selected in the absence of clouds and possibly during the rainy season (to be as close as possible to bankfull flow conditions), for some bends it was difficult to provide a reliable estimate of the channel width, owing to the presence of emerged central bars or of ongoing chute cutoffs. A clear example of these difficulties is reported in Figure 3, showing a couple of bends of the Ucayali River for different flow discharge conditions. Clearly, in order to obtain a reliable along-channel distribution of surface cross-section width, a large enough number of sections were considered in the analysis.

2.2. Statistical Analyses

Two main groups of statistical analyses have been carried out on the width data extracted for each river. The first group concerned the spatial distribution $B(s)$ at a fixed time; the second assessed the temporal variability of this distribution.

For each sequence $B(s)$, the mean B_{avg}, the standard deviation σ_B, the variation coefficient $CV_B = \sigma_B/B_{\text{avg}}$, the minimum B_{min} and maximum B_{max} values, the skewness γ_B, and the kurtosis κ_B were computed. A series

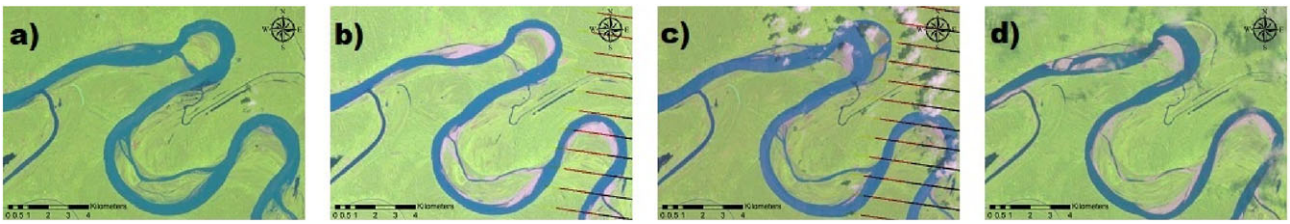

Figure 3. Typical examples of Landsat images of changes in surface channel width observed in the Ucayali River for different flood events: (a) 2005, (b) 2006, (c) 2007, and (d) 2008.

of different PDFs were then fitted to the histogram of $B(s)$. The choice of the PDF that best approximates the histogram was made by using the Bayesian information criterion (BIC), based on the likelihood function (Schwarz, 1978). The criterion was applied to both dimensional and dimensionless half-width data.

The statistical variability of $B(s)$ with time was verified by means of various tests. The analysis of variance (ANOVA) F test and a few multiple range tests (Tukey's test, Scheffe intervals, and Bonferroni intervals) were used to assess whether or not the mean width keeps statistically constant over different years. The ANOVA F test is based on the ratio of between-group mean to within-group mean. Multiple comparisons among all pairs of means (i.e, concerning river planforms observed in different years) have been carried out by means of Tukey's range test (Tukey, 1949). The estimation of all possible contrasts among the means, and not just pairwise comparisons, has been made by using Scheffe intervals (Scheffe, 1999). Finally, the Bonferroni intervals obtained using Bonferroni's inequality were considered to estimate any preselected number of contrasts (Dunn, 1961).

Bartlett's test (Bartlett, 1937) was applied to each river to compare a weighted average of the within-sample variances to their geometric mean. Levene's test (Levene, 1960) was used to perform a one-way analysis of the absolute differences between each observation and its corresponding group mean. The rank-based nonparametric test of Kruskal-Wallis (Kruskal & Wallis, 1952) and the nonparametric Mood's median test (Mood, 1954), a variant of the Pearson's chi-square test, were employed to measure how the central tendency (the median) possibly changes in time.

Finally, the Bhattacharyya coefficient (BC) was computed to quantify the statistical differences between the PDFs fitted to width data observed in different years. In particular, the Bhattacharyya distance coefficient, that is, the negative logarithm of BC, allows one to objectively approach the similarity problem in a geometric sense, identifying the possible overlapping between two distributions (Bhattacharyya, 1943).

2.3. Mathematical Modeling

The present study focuses on the modeling of the middle- and long-term evolution of a meandering river in which not only the planform but also the channel width can vary in time, depending on the subtle interplay between erosion and deposition. The general framework is that recently used by Bogoni et al. (2017) to describe the self-interactions between a river and its surrounding floodplain. Here as a novel feature, we relax the assumption of constant river width. The bank erosion at the outer bank is still driven by the velocity defect at the inner and outer banks of a bend, but erosion and accretion processes are activated independently, depending on two different shear stress thresholds. In addition, these thresholds are such that, for a given range of stresses, erosion and deposition regimes can take place together.

The hydromorphodynamic model used to determine the shear stresses acting at the banks is that developed by Frascati and Lanzoni (2013) for single thread channels, which accounts for both curvature and cross-section width variations. We refer the interested reader to Frascati and Lanzoni (2013) for the details of the model. Here we recall that the model takes advantage of the fact that alluvial rivers often exhibit relatively small curvatures and evident but relatively small width variations. This implies the existence of two small dimensionless parameters, the curvature ratio, $\nu = B_{avg}/R_0$, and the dimensionless intensity of width variations, $\delta = (B_0 - B_{avg})/B_{avg}$, founded upon the mean channel width B_{avg}, the minimum value of the radius of curvature of the channel axis R_0, and the maximum width B_0 within the considered reach. These parameters allow for a linearization of the equations of fluid mass and momentum conservation, parameterized for the centrifugally induced secondary currents, and the sediment balance equation, that are solved perturbatively. The resulting description of the flow field and bed topography is thus strictly valid for wide, mildly curved and long bends in which nonlinear effects of bed perturbations can be reasonably neglected as a first approximation and small enough width disturbances as compared with the mean channel width. The relatively low computational cost required by the solution of the resulting set of equations makes the model suitable for long-term meandering simulations (Camporeale et al., 2007; Frascati & Lanzoni, 2009). The outputs of the model are the in-channel flow and the corresponding topography associated with a prescribed uniform water discharge. The input data are the planimetry of the channel axis s, the along-river half-width distribution $B(s)$, the water discharge Q, the average longitudinal bed slope S of the river reach, and the characteristic sediment grain size d_s. Denoting by D_u the mean flow depth corresponding to the reach-averaged channel width B_{avg}, the equivalent dimensionless parameters are the mean half-width to depth ratio $\beta = B_{avg}/D_u$, the dimensionless sediment grain size d_s/D_u, the Shields parameter for the reference uniform flow, $\tau_{*u} = D_u S/(\Delta d_s)$, and the particle Reynolds number $R_p = (\Delta g d_s^3)^{1/2}/\nu$, with $\Delta = \rho_s/\rho - 1$ the relative immersed density of sediment.

Bank erosion of alluvial rivers usually occurs at bankfull or near-bankfull flow conditions. It is thus an intermittent and heterogeneous process. However, on the slow timescale associated with the planimetric development of the river, erosion and deposition can be considered as contemporaneous events, and consequently, bank erosion may be modeled as a continuous process. In other words, we replace the actual process during floods by an integrated and continuous description on the long-term (Howard, 1992; Ikeda et al., 1981; Lanzoni & Seminara, 2006). Therefore, the bankfull flow conditions are here specifically considered to drive the channel planform evolution. In the present contribution, as a first approximation, we assume also that the floodplain adjacent to the river is homogeneous. The accretion of the inner bend is assumed to depend on the rate of deposition ξ_D of fine material made available by the river, computed through the relation (Mehta & Partheniades, 1975)

$$\xi_D = M_D \left(\frac{\tau_D - \tau}{\tau_D} \right) \tag{3}$$

with M_D the deposition rate coefficient, selected on the basis of field data. Here τ is the near-bank shear stress, and τ_D is the critical shear stress for deposition. For the sake of simplicity and as a first approximation, M_D is taken as constant. In addition, τ_D is assumed as the shear stress for which all the sediment is entrained in suspension. This choice of τ_D implies that, in principle, it could exist an interval of bed stresses for which deposition can coexist with erosion, which is assumed to begin when the shear stress equals the value $\tau_E (< \tau_D)$ for incipient particle movement. Different studies have been made to determine the relation between the shear velocity and the settling velocity of sediment (see, among many others, Celik & Rodi, 1991; Cheng & Chiew, 1999; Van Rijn, 1984). In the present context, the probabilistic approach proposed by Bose and Dey (2013) has been adopted (see Appendix A).

The erosion rate ξ_E at the outer bank is estimated through an excess threshold linear formula of the form (Darby et al., 2002; Motta et al., 2012)

$$\xi_E = M_E \left(\frac{\tau - \tau_E}{\tau_E} \right), \tag{4}$$

where M_E is an erosion rate coefficient (dimensional) and τ_E is the critical shear stress threshold over which erosion occurs (see Appendix A). This treatment of bank erosion does not account for the sheltering effect due to the presence of cohesive slump blocks (Parker et al., 2011). Although it is possible to relax this assumption, we choose to reduce as much as possible the number of parameters by considering the armoring effect of slump blocks implicitly, that is, embedding it in the statistical description of channel width variations described below.

The idea is that a given river reach can be characterized through a PDF of the cross-section channel width (specifically, a GEV distribution) embedding in an integral sense the intrinsic features of the considered reach and of the surrounding floodplains. The parameters of this river-specific PDF can generally vary in time, especially after significant changes of the river planform (e.g., after cutoff events). However, on average, they tend to attain almost constant values, depending on the hydrological regime of the river, the sedimentological characteristics of the transported sediment, of the river banks, and of the surrounding floodplain. We propose to use this characteristic PDF to constrain the channel width variations as the river migrates through the floodplain. The cumulative density function (CDF) of the selected PDF is assumed to describe the spatial distribution of channel width. The rate of erosion at the outer bank ξ_{BE} and deposition at inner bank ξ_{BD} are thus computed as

$$\xi_{BE} = \xi_E R_E, \qquad \xi_{BD} = \xi_D R_D \tag{5}$$

where the correction factors R_E and R_D are such that

$$R_E = \begin{cases} 1 & \text{CDF} \leq 0.5 \\ 2\,(1 - \text{CDF}) & \text{CDF} > 0.5 \end{cases} \tag{6}$$

$$R_D = \begin{cases} 1 & \text{CDF} \geq 0.5 \\ 2\,\text{CDF} & \text{CDF} < 0.5 \end{cases} \tag{7}$$

This statistical approach has two aims. The first is to connect the two banks, by favoring or restricting the bank movement as a function of the CDF and of the mean channel width. The second is to set lower and upper limits to the channel width, thus avoiding extreme, nonphysical width values during the river evolution. The multiplicative coefficients provided by relations (6) and (7) ensure that bank retreat/accretion processes tend

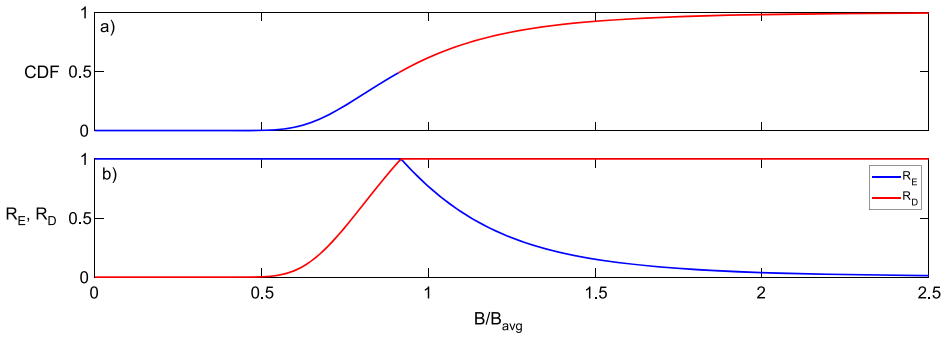

Figure 4. (a) Cumulative density function of $B(s)/B_{avg}$ and (b) the corresponding correction factors (6) and (7) computed for the general extreme value distribution fitted to the cross-section width data observed for the Ucayali River (year 1998). CDF = cumulative density function.

to be frozen when the width attains too small or too large values. In this way, the bank movement governed by the physical rules embodied by equations (3) and (4) is corrected in a statistical sense through equation (5). A typical example of the CDF of $B(s)/B_{avg}$ and of the corresponding coefficients R_D and R_E is shown in Figure 4, referring to the Ucayali River (see section 3). It clearly appears the different behaviors of the two correction factors, as well as the width extremes (∼0.5 and ∼2.5) below and above which the retreat/accretion processes tend to stop.

The procedure followed to determine the evolution of the channel width can be summarized as follows. The channel is divided in N sections located at distances Δs_i^j along the channel axis s. Here the subfix i refers to the time step, while the apex j defines the channel cross section. At each time step Δt_i, the erosion and accretion rates (ξ_E and ξ_D) are computed separately for each bank using the relation

$$\xi_{B_{l,r}} = (\xi_{BE} - \xi_{BD})_{l,r}, \tag{8}$$

where the subfixes l and r denote the left and right banks, defined with respect to the flow direction. Note that, as discussed above, in principle, it could exist an interval of bed stresses for which deposition can coexist with erosion, depending on the values attained by τ_E and τ_D. That is why erosion and deposition rates are computed at both banks. Clearly, the possibility that erosion and deposition coexist or not at a bank depends on the value actually attained by the shear stress τ.

Next, the rate of displacement of the channel axis points is determined as

$$\xi = \xi_{B_l} - \xi_{B_r}. \tag{9}$$

The channel axis is defined as the locus of points with mean distance between the two banks. The displacements of these points are computed as

$$x_i^j = x_{i-1}^j - \Delta t_i \, \xi_i^j \sin\theta_i^j \tag{10}$$

$$y_i^j = y_{i-1}^j + \Delta t_i \, \xi_i^j \cos\theta_i^j. \tag{11}$$

In the absence of the armoring action exerted by slump blocks, the time step Δt_i can vary during the computations. Several simulation tests suggested to select the time step according to the relation

$$\Delta t_i = \frac{2\,\Delta s_i}{\max\left(M_E, M_D\right)} \tag{12}$$

in order to ensure stable computations. Since only the central axis is displaced, the width changes for each cross section are computed as

$$B_i^j = B_{i-1}^j + \frac{1}{2}\left(\xi_{B_l} + \xi_{B_r}\right)_{i-1}^j \Delta t_i \tag{13}$$

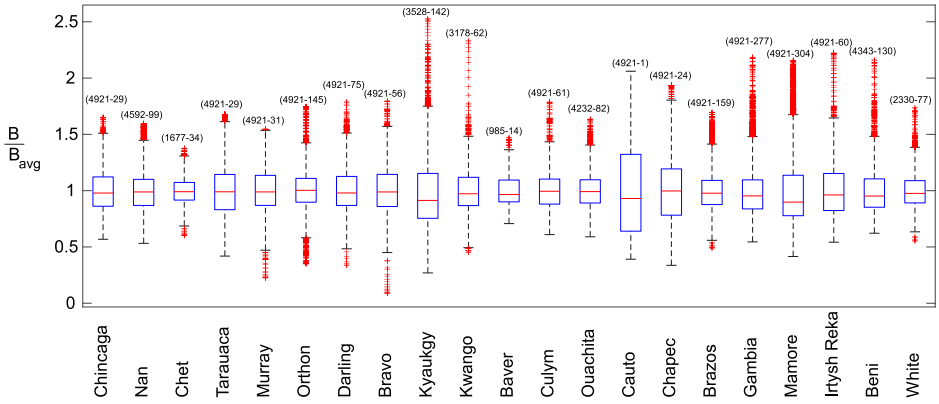

Figure 5. Box and whisker plots computed for the along-channel distributions of the dimensionless half-width $B(s)/B_{avg}$, observed in the considered rivers. The numbers in the upper part of the plot, delimited by round brackets, denote the size of the sample and the number of outliers.

After the new meandering configuration is computed, all the input data to the hydraulic model are updated. By considering as fixed the elevations at the upstream and downstream ends of the channel reach (i.e., a constant Δz), the new average values of channel slope, flow depth, and flow velocity result

$$S_i = \frac{\Delta z}{L_i} \tag{14}$$

$$D_{ui} = \left(\frac{C_f Q^2}{4 B_{avg}^2 g S} \right)_i^{1/3} \tag{15}$$

$$U_{ui} = \left(\frac{g Q S}{C_f 2 B_{avg}} \right)_i^{1/3} \tag{16}$$

with L_i the intrinsic length (i.e., measured along the curvilinear coordinate s) of the channel axis. This procedure is repeated at each time step. When L_i experiences a change larger than 10% of its original value (e.g., an abrupt shortening because of a neck cutoff or an elongation due to channel migration), new nodes are added to maintain the size of the spatial step Δs_i in the range 0.9–1.1, and a standard cubic spline interpolation is used to remesh the points uniformly along the channel axis.

3. Results

3.1. Spatial Distribution of Channel Half-Widths

The results of the statistical analysis carried out on the sequences of $B(s)$ extracted for each river are summarized in Table 1. The coefficient of variation CV_B varies in the range 12.7–44.5%, with a mean value of 23.6 and a median value of 20.4. The higher values are observed for longer river reaches (Chapec, Gambia, Irtysh Reka, Mamore, and Ucayali) or located in the proximity of a delta region (Bravo, Cauto, and Kyaukgy). Overall, the statistical parameters of Table 1 suggest that $B(s)$ does not follow a normal PDF. This is confirmed by the comparison among the entire set of rivers shown in Figure 5 and reporting the box and whisker plots of the dimensionless half-channel widths. The boxes represent the interquartile ranges corresponding to the 50% of the data; the horizontal line within each box denotes the median; the whiskers extend up to 1.5 times the interquartile range. All the values outside the whiskers are considered as outliers. From Figure 5, it clearly appears that for almost all the rivers the line representing the median is not located in the center of the boxes, and hence, the mean and the median do not coincide. In addition, even though the median in general varies within a relatively limited range (0.904 to 1.013), the whiskers tend to differ significantly from river to river. Finally, the data falling outside of the whiskers concentrate mainly in the upper whisker. Only the Cauto River does not present any data outside of the whiskers but has a quite high extension of the upper whisker. The larger outlier values are found for the Kyaukgy River, while the Bravo River exhibits the smaller outlier values. Finally, the Chet River is characterized by the most compact box and has whiskers of almost equal length.

The application of BIC, applied to both dimensional ($B(s)$) and dimensionless ($B(s)/B_{avg}$) half-width sequences, indicates that in most of the cases a GEV distribution provides the best data fitting. Note that, when comparing

Table 1
General Statistics of Half-Width Distributions B(s) for the Rivers Shown in Figure 1

No.	River	Sample size	B_{avg} (m)	σ_B (m)	CV_B (%)	γ_B (—)	κ_B (—)
1	Chincaga	4,921	39.86	7.33	18.40	11.62	−2.78
2	Nan	4,592	46.44	8.51	18.31	14.45	5.03
3	Chet	1,677	21.66	2.75	12.71	4.72	1.08
4	Tarauaca	8,496	75.47	18.11	23.99	11.86	−1.03
5	Murray	5,222	47.45	9.21	19.40	0.32	3.06
6	Orthon	18,261	45.6	7.95	17.43	13.49	34.11
7	Darling	8,699	15.55	3.14	20.21	20.03	11.92
8	Bravo	12,688	20.19	8.98	44.46	104.57	162.76
9	Kyaukgy	3,528	24.24	8.60	35.48	28.37	15.09
10	Kwango	3,178	24.87	5.12	20.60	22.09	39.5
11	Baver	985	19.31	2.77	14.33	8.64	1.14
12	Culym	6,953	107.24	19.62	18.29	10.09	17.81
13	Ouachita	4,232	47.66	7.60	15.95	14.28	10.43
14	Cauto	5,564	50.14	20.23	40.34	11.80	−12.67
15	Chapec	16,547	256.04	82.66	32.28	30.22	1.42
16	Brazos	12,058	64.26	11.18	17.39	37.32	30.3
17	Gambia	17,948	59.47	16.42	27.61	134.19	327.14
18	Mamore	11,742	168.78	48.33	28.63	72.76	85.77
19	Irtysh Reka	8,585	164.93	44.36	26.90	43.64	46.6
20	Beni	4,343	227.06	47.88	21.09	39.96	48.87
21	White	2,230	88.19	14.36	16.29	19.39	19.32
22	Bermejo[2]	7,306	120.56	25.12	20.84	0.74	3.78
23	Chixoy[4]	1,057	76.21	14.94	19.60	0.55	3.18
24	Sacramento[4]	5,153	75.07	13.52	18.01	0.76	4.36
25	Segovia[2]	10,350	105.85	21.08	20.67	1.32	7.32
26	Ucayali[32]	4,159	421.74	186.4	44.20	1.75	6.67

Note. All river configurations were taken in 2016 expect for the Chixoy (1986), the Sacramento (1994), and the Ucayali (2014). The superscript at the end of the river name denotes the number of planform configurations considered for studying the spatiotemporal distribution of channel half-width.

the best fitting PDFs, the differences in BIC values are larger when considering the dimensionless data, since the normalization by B_{avg} amplifies the sensitivity to any variation. Only for 2 out of 26 rivers and 65 investigated configurations, the GEV distribution is not among the first three best fitting PDFs. These two rivers (Kwango and Orthon) do not present any particular different feature with respect to other rivers located at similar latitudes, for which the GEV yields the best fitting.

Some typical examples of the river half-width histograms and the first two best fitting PDFs are depicted in Figure 6. In a few cases (e.g., the Cauto) the width histogram presents a bimodal distribution. This behavior is related to the presence of a drastic change in the geometry of the river (Figure 2a), possibly driven by significant variations in flow discharge, bed slope, or backwater effects. Even for this type of histogram, the GEV is the PDF (among those investigated) that ensures the best data fitting. Another peculiar case is represented by the Beni River, for which the GEV adapts nicely to the observed histogram, even if the river width undergoes large variations (Figure 2c). Finally, it is worth to mention that the rivers that are better described by a river-specific PDF (e.g., the GEV) are those with long enough reaches (i.e., with a large enough number of sampled cross sections), located far enough from the sea and without significant tributaries.

3.2. Spatiotemporal Distributions of Channel Widths

The results of the previous section suggest that different meandering rivers all around the world have similar PDF distributions of channel half-widths. The modeling of meandering river evolution requires to know

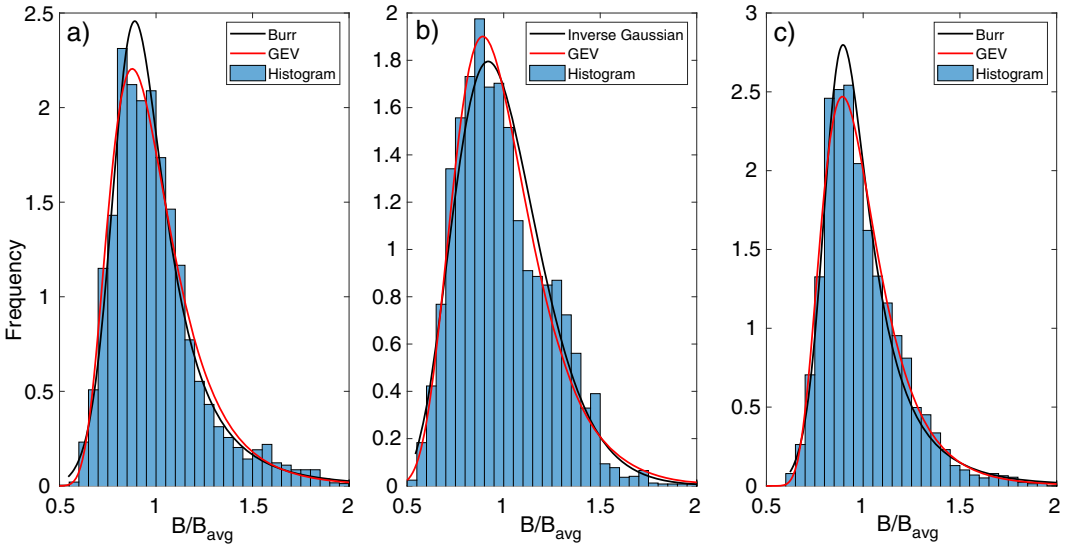

Figure 6. Typical examples of the histograms, of the probability density functions ensuring the first and second best fitting, and of the GEV distribution for dimensional channel half-width data. (a) Gambia, (b) Irtysh Reka, and (c) Beni Rivers. GEV = generalized extreme value.

whether or not these PDFs undergo variations as the river migrates throughout the floodplain. To answer this question, the planforms of five rivers (Bermejo, Chixoy, Sacramento, Segovia, and Ucayali) have been analyzed at different times. The planforms of the Chixoy and Sacramento Rivers were extracted from images taken before and after chute cutoff events. In the case of the Sacramento high spatial resolution images corresponding to the more recent years were available. For the Bermejo and Segovia Rivers, the considered planforms have been selected randomly among those available. Due to a large amount of accessible data, the Ucayali River is discussed separately.

The general statistics concerning the spatiotemporal sequences of half-width data observed in these rivers (see Table S2 in the supporting information) suggest that, in general, the best fitting PDF does not change significantly as a river moves across the floodplain. This hint is confirmed by the box and whisker plots shown in Figure 7. Remarkable similarities are displayed by the half-width distributions observed in the Segovia River after a time interval of 17 years. More significant width fluctuations characterize the Bermejo River (during a time interval of 14 years), the Chixoy River (during three different time intervals, spanning in total 30 years), and the Sacramento River (during two different time intervals, spanning in total 20 years).

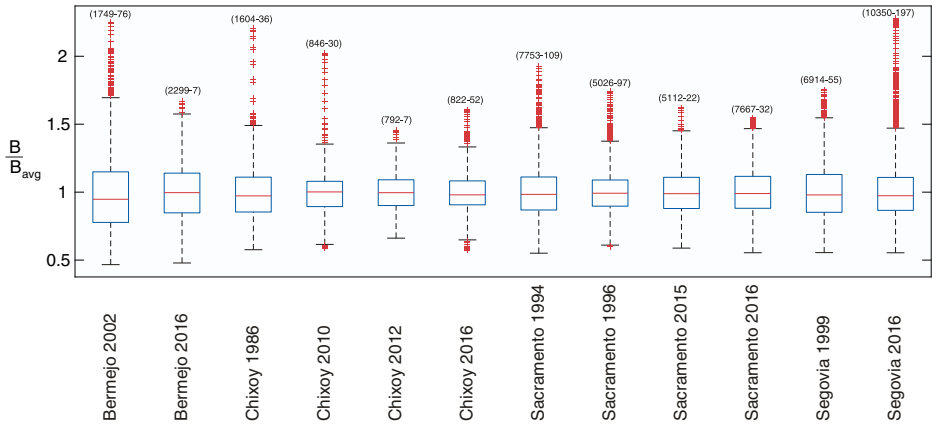

Figure 7. Box and whisker plots computed for the along-channel distributions of the dimensionless half-width $B(s)/B_{avg}$, observed in different years for the Chixoy, Sacramento, Bermejo, and Segovia Rivers. The numbers in the upper part of the plot, delimited by round brackets, denote the size of the sample and the number of outliers.

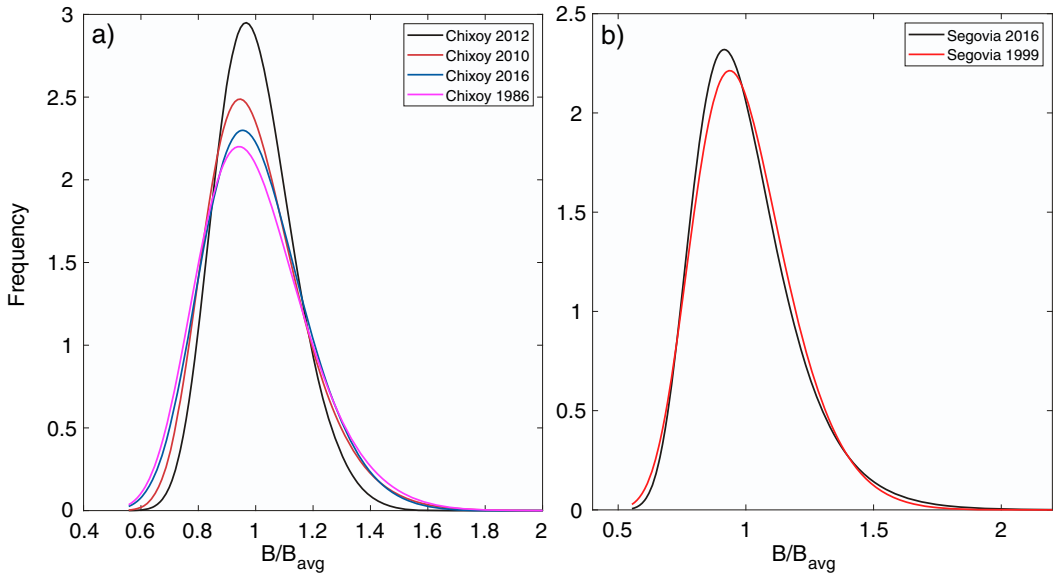

Figure 8. Typical examples of the temporal variations experienced by the generalized extreme value probability density distribution fitted to dimensionless $B(s)/B_{avg}$) distribution observed in the Chixoy (a) and Segovia (b) Rivers in different years.

The statistical tests (ANOVA, Tukey's test, Scheffe, and Bonferroni intervals) indicate that the half-width mean usually changes throughout years at a 95% confidence level. The tests for variance check (Bartlett and Levene) reveal a similar behavior. Just in three cases, the variance did not vary appreciably throughout years. Nevertheless, the tests (Kruskal-Wallis and Mood) performed to analyze how the median tendency possibly changes over time suggest that all the investigated rivers, except the Bermejo, do not exhibit significant variations.

The deduction that the cross section width fluctuates around a statistically stationary state as the river planform continuously evolves is confirmed by the variations exhibited throughout years by the parameters of the best fitting PDFs (e.g., Figure 8). In the absence of significant shortening of the river planform consequent to cutoff processes, the changes in parameters are relatively small, in particular, when considering dimensionless half-width sequences. It also clearly appears that, even though evident departures from similarity are observed just after cutoff events, later on the river tends to progressively recover a PDF distribution of channel width similar to the preevent one. The BC confirms the behavior emerging from Figure 8 (see Table S3 in the supporting information). Indeed, the lower values of BC are attained for the configurations before and after chute cutoff events, while for the rest of the period of observation the BC values suggest a relatively high degree of similarity, especially when considering dimensionless data. Only the Sacramento River shows values of BC below 0.97.

These findings reinforce the idea that as the river meanders throughout the floodplain, its width oscillates around an equilibrium value, and the corresponding probability density distribution is described by a PDF distribution with well-defined parameters that keep almost constant in time. The values attained by these parameters are in fact dictated by the water and sediment discharges externally supplied to the river, as well as by the average sedimentological and stratigraphic characteristics of the river banks and of the surrounding floodplain.

To further substantiate the hypothesis of the existence of a river-specific GEV distribution of channel half-width, we now consider in detail the case of the Ucayali River. Figure 9 shows the erosion and deposition data, averaged yearly over the entire river reach (133 km long) and spanning an interval of 32 years. The cycles of erosion and accretion (Figure 9a) and the strict correlation between them (Figure 9b) are evident. A weakening of this correlation, however, seems to start after 1995, likely owing to a massive artificial chute cutoff induced downstream of the considered reach. Figure 9c indicates that erosion and accretion time cycles are strictly connected (as expected) to channel width oscillations. The changes in B_{avg} range from a few meters to almost 50 m from 1 year to another, with a coefficient of variability around 30% for nearly all the considered years. The first two largest values of B_{avg} were registered in 2012 and 2007. These extreme values, however,

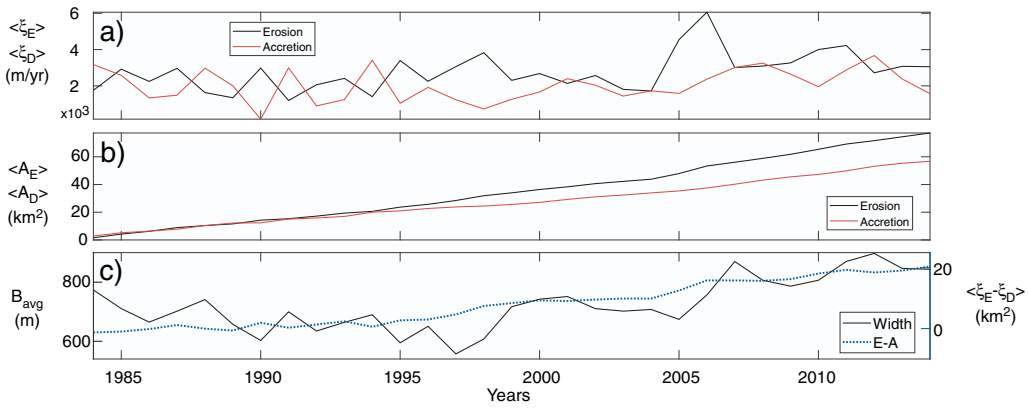

Figure 9. Temporal distribution of the (a) erosion $\langle \xi_E \rangle$ and deposition $\langle \xi_D \rangle$ rates, (b) cumulative erosion $\langle A_E \rangle$ and deposition $\langle A_D \rangle$ areas, and (c) reach-averaged width B_{avg} and the difference $\langle \xi_E - \xi_D \rangle$ observed in the Ucayali River during the period 1984–2015. The operator $\langle \ldots \rangle$ denotes the average along the river reach and over a year. Graphics are obtained by using the software RIVMAP (Schwenk et al., 2017).

should be considered carefully. The Landsat images show that in the correspondence of a bend the river reenters into an old channel bed, and it is difficult to define the correct river width. Consequently, some outliers could have been introduced in the data set. In any case, the standard deviation and the kurtosis are out of the ranges typical of a normal probability density distribution.

An overall view of the statistical behavior of the sequences of $B(s)/B_{avg}$ observed in the various years is given in Figure 10, showing the corresponding box and whisker plots. Of particular interest is the year 2007, when the outliers are particularly numerous. In this year the reach was subject to important elongation and, consequently, experienced high migration rates, leading to the most significant difference between erosion and accretion rates (Schwenk et al., 2017). Such behavior is likely related to the neck cutoffs that occurred in the years 2005 and 2006 that determined the removal of significant meander loops (28 and 9.6 km long, respectively; Schwenk & Foufoula-Georgiou, 2016).

According to the ANOVA test, the 32 annual planforms of the Ucayali River display statistically significant differences of B_{avg} at the 5% significance level. The Tukey's test and the Bonferroni intervals (see Figure S1 in the supporting information), applied to the 496 possible combinations of the river planforms (C_{32}^2 combination without repetitions), detected the same number of couples (439) with a statistically significant difference of B_{avg}. This number decreased to 362 by applying the Sheffe intervals. Nonetheless, for all the tests, a clear difference emerges for the data before and after 2006. Note that, according to the Sheffe intervals, 2005 is the year with the higher number of couples without differences, followed by the years 1985 and 2004. The Tukey's

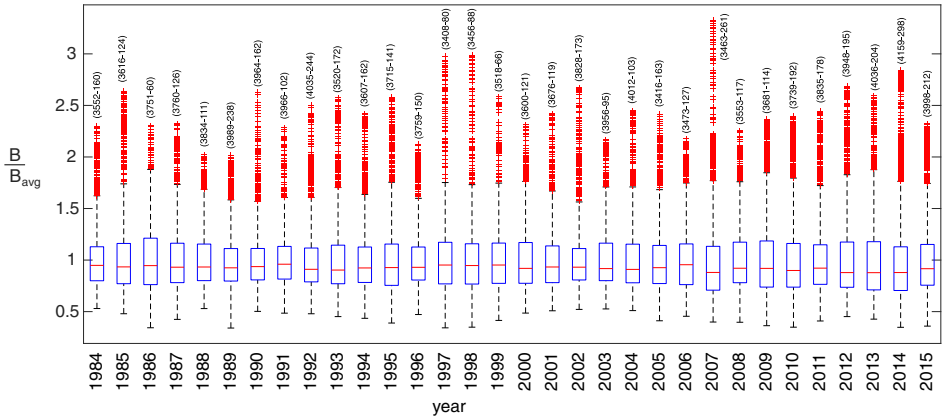

Figure 10. Box and whisker plots computed for the along-channel distributions of the dimensionless half-width data $B(s)/B_{avg}$ observed in different years for the Ucayali River.

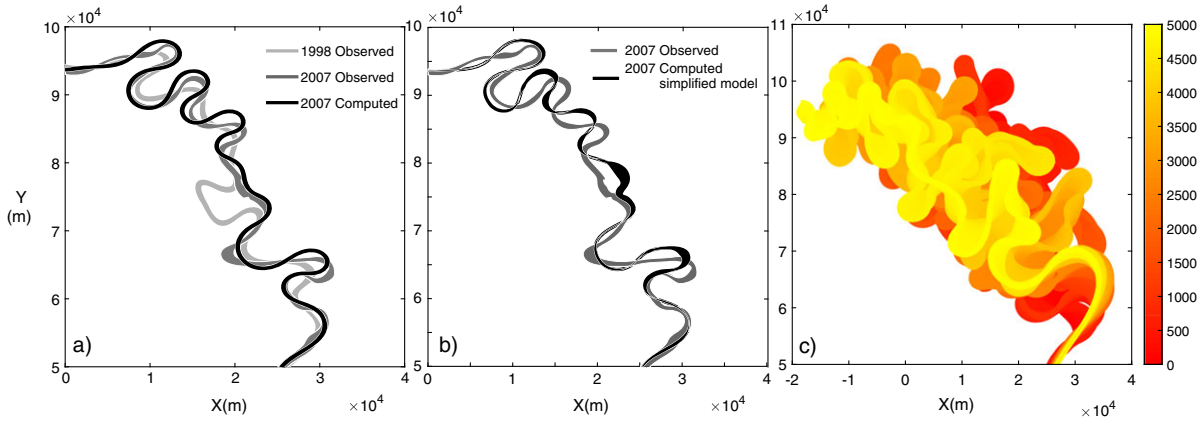

Figure 11. (a, b) Short-term (10 years) and (c) long-term (5,000 years) simulations of planform evolution experienced by a reach of the Ucayali River. Panel (a) shows the observed initial and final configurations and the planform computed with the flow field accounting for along-channel width variations and employing the statistical constraint on the temporal width evolution (full model). Panel (b) shows the observed final configuration and the planform computed with the flow field assuming a constant channel width and without considering statistical constraint on width evolution. The color vertical bar in panel (c) indicates the year of simulation carried out with the full model. The mean values of the curvature ratio and the dimensionless intensity of width variations in the investigated reach are $\nu = 0.381$ and $\delta = 0.522$.

test and the Bonferroni intervals give similar results, with the highest number of couples without differences in the years 1985, 1987, and 2004.

The statistical behavior of the variance is very similar to that of the mean. The Bartlett and Levene tests point at statistically significant differences between the variances in most of the couples of years (404 couples out of 496). Similar to the case of the mean, the variance tests highlight the existence of two groups of data, before and after 2006. The year 1984 presents the larger number of couples without differences, followed by 2005.

Also, in the case of the Ucayali, the GEV is the distribution that ensures the best fitting (for 30 of the 32 examined planforms). Even in the 2 years for which the GEV does not yield the best fitting, the differences with the optimal PDFs are quite small (less than 0.05% when considering dimensional half-width data). The appropriateness of the GEV distribution to describe the spatial distribution $B(s)$ is confirmed by the high values (larger than 0.99) attained by the BC independently of the considered year. This tendency is recovered also varying the number of sections used to sample $B(s)$ (the cross-section distance being varied in the range 10–700 m, with the upper limit dictated by the mean channel width). The BC values suggest that the lower similarity is attained for the years 1997 and 2012 ($BC = 0.752$) for $B(s)$ and in years 1988 and 2014 ($BC = 0.936$) for $B(s)/B_{avg}$. Some important morphological changes occurred during these years. The biggest was in 1997 and consisted of a human-induced chute cutoff that removed a 72-km bend loop, just a few kilometers downstream of the investigated river reach. A chute cutoff of natural origin took place in 2012. Owing to the shorter length of the bypassed loop (about 11 km), the changes experienced by the river width are less important than those attained after the 1997 cutoff but still significant.

3.3. Modeling Results

Figure 11 shows the results of a short-term (10 years) and a long-term (5,000 years) simulation carried out for the reach of the Ucayali River analyzed in Figure 9. The reach is 133 km long and has a mean slope of about 3.3×10^{-5} m/m (assumed similar to that between Pucallpa and Tiruntan; H&O - ECSA, 2005). The statistical analysis of the width data extracted in 1997 yields $B_{avg} = 313$ m, corresponding to a width to depth ratio $\beta = 30$ (Ettmer & Alvarado-Ancieta, 2010). The CDFs to be used in equations (6) and (7) are those obtained from the observed data and depicted in Figure 4. The values of the erosion and deposition coefficients $M_E = 215$ m/y and $M_D = 189$ m/year (equations (3) and (4)) are those corresponding to the mean of the values shown in Figure 9. In addition, τ_D and τ_E have been set equal to 1.07 and 5.79 N/m^2, respectively; see Appendix A. These input parameters are used to eventually compute the ξ_{BE} and ξ_{BD} values for each time step of the channel axis evolution.

The temporal interval chosen to test the model in the short term is that from 1997 to 2007, during which a neck cutoff was observed inside the reach. Despite the model limitations dictated by its linearized character and by the assumptions of constant discharge, homogeneous sediment, and constant floodplain erodibility,

Table 2
Dissimilarity Index d Computed Through Procrustes Analysis Characterizing the Comparison Between the Configuration of the Ucayali River Observed After a 10-Year Interval (see Figure 11) and the Planforms Computed by Employing the Complete Model and a Number of Its Simplified Versions

Model	d_{LB}	d_A	d_{RB}	$\hat{B}_{avg}$	$\hat{B}_{med}$
Variable width flow, with statistical constraint	0.0073	0.0073	0.0094	0.77	0.81
Variable width flow, without statistical constraint	0.0108	0.0101	0.0117	0.46	0.74
Constant width flow, with statistical constraint	0.0080	0.0079	0.0099	0.69	0.73
Constant width flow, without statistical constraint	0.0104	0.0100	0.0112	0.44	0.36

Note. The comparison has been carried out on the lines describing the left bank (LB), the axis (*A*), and the right bank (RB) of the channel. The last two columns report the mean value, $\hat{B}_{avg}$ and median value $\hat{B}_{med}$ of the simulated channel width, divided by the corresponding quantities (B^{obs}_{avg} and B^{obs}_{med}) observed in the considered reach.

after 10 years the simulated planform appears to reproduce with an acceptable degree of approximation the observed river path, as well as the spatial width fluctuations (Figure 11a). The most significant discrepancies between observed and computed configurations are obviously attained for the sharpest bends, for which linearization fails (Frascati & Lanzoni, 2013).

The results of the long-term simulation (Figure 11b) indicate that the computations keep stable in terms of channel width variations, always yielding physically reasonable values of the mean channel width. The river moves inside the entire meander belt from left to right, leaving behind a large number of oxbow lakes.

In order to verify objectively the performance of the model, we carried out some additional short-term simulations by employing simplified versions of the model, namely, (i) keeping constant the cross-section width along the channel and letting it vary in time without imposing any statistical constraint, (ii) letting the channel width to vary along the channel and in time but not imposing any statistical constraint, and (iii) keeping constant the width along the channel but letting it to vary in time applying the statistical constrain. The configurations resulting after 10-year simulations have been compared objectively with the planform observed in the Ucayali River through a procrustes analysis (Dryden & Mardia, 2016). Each element (axis line, left bank, and right bank lines) of a computed planform has been linearly transformed (through translation, reflection, orthogonal rotation, and scaling) to best conform it to the corresponding counterpart in the observed configuration. The minimized sum of squared errors is taken as a goodness-of-fit criterion (dissimilarity index *d*) and measures the dissimilarity between the two planform patterns. The dissimilarity indexes obtained in the various type of simulations are shown in Table 2 and indicate that the better agreement between simulated and observed planforms is indeed obtained by accounting for the effects of width variations on the flow field and constraining statistically the channel width as it evolves in time owing to the combined action of erosion and deposition at the river banks. Considering a constant width flow field but including the statistical constraint leads to slightly worse results. Neglecting completely these effects decreases significantly the performance of the prediction. The introduction of the statistical constraint described in section 2.3 is thus fundamental to improve the reliability of predictions. These conclusions are confirmed by the mean and the median values of the computed widths, normalized by the reach-averaged observed width, that are also reported in Table 2.

4. Discussion

The statistical comparison among sequences of channel half-width observed in different rivers suggests a common behavior, with a relatively low number of data that depart from the general tendency (the outliers of Figures 7 and 10). This behavior is common to an extensive set of rivers all around the world, with different hydrological regimes, type of soils, and land uses. Consequently, the present study is deemed to entail a wide range of applicability. In particular, the GEV is the PDF that more frequently better describes the sequence of along half-width channel data.

It is also remarkable what the statistics reveal about the evolution of river width throughout years, in particular, in the case of the Ucayali River, for which a long record of data is available. In general, the mean channel half-width B_{avg} does not remain constant in time, and its fluctuations are significant from a statistical point of view. However, even if a river continuously tends to modify its cross-section geometry and, therefore, to change its half-width statistics as a result of planform evolution, the fluctuations are limited to some specific

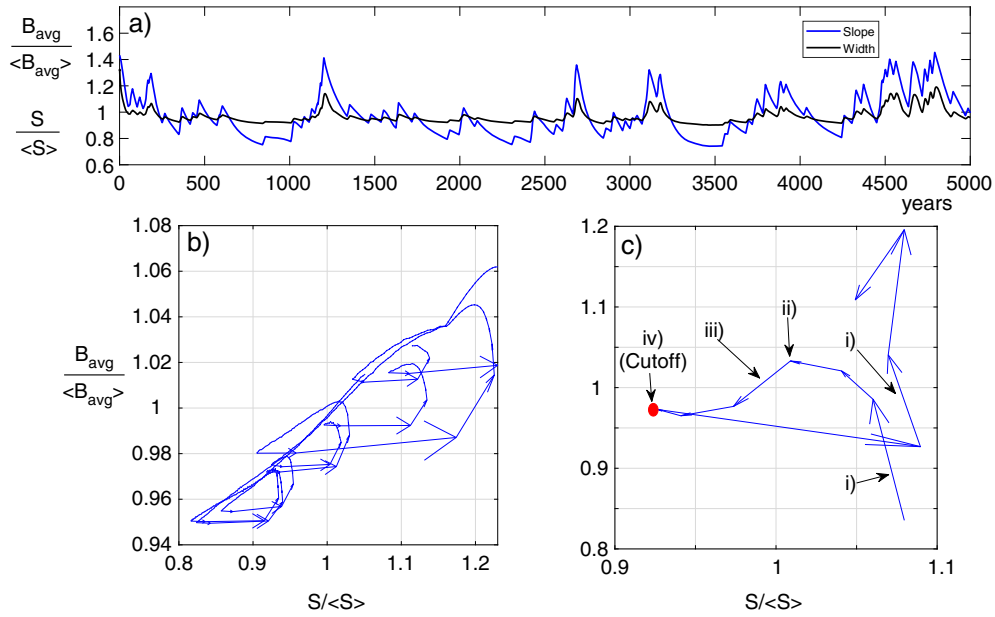

Figure 12. (a) The mean channel width B_{avg} and the reach slope S (equation (14)) are plotted versus the time t. Both the variables are normalized with their temporally averaged values, $\langle B_{avg} \rangle$ and $\langle S \rangle$. (b, c) Temporal trajectories of the B_{avg}-S relation resulting from (b) the long-term simulation of Figures 11c and (c) observed in the Ucayali River for a neck cutoff. The black arrows, labeled with (i), (ii), (iii), (iv), and again (i), indicate some relevant moments of the looping cycle.

intervals. In other words, for a given river B_{avg} tends to fluctuate within a relatively limited range of values. Moreover, in most of the cases the couple of years for which B_{avg} does not present statistically significant differences are not consecutive. This behavior has motivated the physics-statistics-based mathematical model described in section 2.3, grounded on the assumption of a river-specific PDF distribution of $B(s)$.

The modeling framework developed here appears to produce reliable estimates of the short-term evolution of a given river reach and, in the long term, a reasonable picture of the floodplain occupation by the river. Clearly, the robustness of these predictions requires that the governing equations can be actually linearized; that is, the considered river bends are wide, mildly curved, and long, and the along-channel width variations are small enough with respect to the mean channel width.

The long-term numerical simulations also provide some insight into a peculiar behavior displayed by the mean channel width when plotted as a function of the channel slope. Figure 12a displays the strong correlation existing between B_{avg} and S resulting from the simulation. At any change in slope, it corresponds a change in mean channel width, in some cases with a small time lag. The temporal trajectories of the B_{avg}-S relation (Figure 12 b) in general exhibit looping cycles, characterized by an initial relatively rapid increase up to a maximum, followed by a decrease, until the mean reach slope grows abruptly. This particular shape of the trajectories can be explained as follows. The channel width is computed by considering separately erosion of the outer bank and accretion of the inner bank. The shear stresses responsible for these processes depend on the velocity and, ultimately, on the slope. A lower slope implies a smaller mean flow velocity. This dynamics is strongly influenced by the occurrence of cutoffs (in the present model just neck cutoffs). Indeed, each cutoff event produces a sudden growth in-channel slope, with a consequent increase of the mean flow velocity and, hence, of the erosional power. The subsequent evolution of the channel is characterized by a progressive elongation, with a reduction of the slope and a widening of the cross section (i — phase in Figure 12c). This trend continues until a maximum width is attained when erosion and deposition processes at the banks nearly balance (ii — moment in figure 12c). Later on, deposition prevails over erosion, leading to a narrowing of the channel cross section, while the slope continues to reduce owing to channel axis elongation (iii — phase in Figure 12c). Eventually, neck cutoff conditions are achieved (iv — moment in Figure 12c) and a looping trajectory starts again in a different position of the B_{avg}-S plane. Note that in this plane the looping trajectories associated to different cutoffs tend to localize below a straight line (Figure 12b) whose inclination depends

on the values of τ_E and τ_D. Essentially, as the channel elongates decreasing its slope, the interplay between erosion and deposition at the channel banks (controlled by τ_E and τ_D) constrains the channel width ($B \propto \xi_E - \xi_D$) in the lower triangular portion of the B_{avg}-S plane, as depicted in Figure 12b.

The simulations also reveal that in a few occasions (especially for low channel slopes) the river tends to attain a quasi-stable configuration, with very slow bank displacements and shear stress values close to the critical thresholds for erosion and deposition. Just a sudden morphological change, as induced by a cutoff event, can break this pseudoequilibrium, by changing the slope and forcing the river width to attain a new stable value.

5. Conclusions and Future Developments

We used Landsat images to investigate the statistical behavior of the distribution of cross-section half-width, $B(s)$, observed along different rivers all over the world and, for a given river, considering different years. A number of statistical measures have been computed and tested to clarify if the observed changes in river width are statistically significative and can be explained by a simple statistical model. Our main conclusions can be summarized as follows.

For each river configuration, the channel half-width invariably fluctuates along the channel. In general, the median of the normalized half-width $B(s)/B_{avg}$ varies within a relatively limited range (0.904 to 1.013), while the interquartile range can differ significantly from river to river and, for a given river, can change throughout years. The mean (i.e., reach averaged) half-width, B_{avg}, usually changes in time, depending on the planform attained by the river as it migrates across the floodplain. Nevertheless, these fluctuations are usually centered around a statistically steady value. This value is a signature of the hydrological and sedimentological regimes characterizing the river, of the overall strength of the banks, and of the sedimentary structure of the surrounding floodplain.

The GEV probability distribution turns out to most often provide the best fit of half-width data. Even though the three parameters controlling the GEV shape usually change from year to year, the differences of the statistical distances between each distribution keep relatively limited, thus implying an almost complete similarity of the distributions. Significant variations in the GEV parameters are observed when the river undergoes significant morphological changes, such as those due to the occurrence of cutoffs. However, a few years after these changes, the GEV parameters tend to recover the preexisting values that can thus be taken as river specific.

We used these observational findings to develop a physics-statistics-based model describing the coupled evolution of the planform channel migration and of the along-channel width. The outer bank erosion and the inner bank accretion are treated separately, thus giving rise to spatial width fluctuations with respect to the mean when the river meanders across the floodplain. These fluctuations are constrained within a meaningful range of values using the GEV distribution that better fits the spatiotemporal sequences of $B(s)$ observed for the investigated river. This river-specific characterization of along-channel width fluctuations is coupled with an already existing linearized model for determining the in-channel bed topography and the corresponding flow needed to compute the rates of bank retreat and accretion.

The short- and long-term simulations carried out with reference to a reach of the Ucayali River confirm the ability of the proposed approach to simulate realistically the coupled evolution of the river planform and of the corresponding cross-section width variations. The computations also suggest the existence of a strict relationship between the mean channel slope and the average channel width. Specifically, the width-slope trajectories are characterized by the presence of looping cycles. The channel width first increases up to a maximum, then decreases as the slope lowers owing to the progressive channel elongation, until a cutoff shortens the channel, leading to an abrupt decrease of the slope. This behavior nicely resembles that observed in a reach of the Ucayali River. The long-term simulations reveal that these looping cycles can also produce quasi-steady planform configurations, with very slow bank displacements, low slope, and high sinuosity.

Finally, we point out that the present treatment of channel width evolution, when needed, can be coupled with any other model of in-channel flow, thus overcoming the intrinsic limitations of the linearized model here adopted, requiring wide, mildly curved, and long bends and small enough width disturbances as compared with the mean channel width.

Appendix A

In this appendix, we report the expressions used for estimating the critical shear stresses for sediment erosion at the outer bank and sediment deposition at the inner point bar. Many different approaches exist to estimate when sediment particles begin to be entrained by a flowing current. The threshold of incipient sediment movement can be in general expressed by considering either the flow velocity (Beheshti & Ataie-Ashtiani, 2008; Simoes, 2014; Yalin, 1963) or the bed shear stress. In this latter case, the proposed relations are of empirical (Kramer, 1935) or semiempirical (Brownlie, 1981; Parker et al., 2003, 2011; Shields, 1936; Soulsby & Whitehouse, 1997; Van Rijn, 1984) origin. Probabilistic and turbulence-based approaches (Ali & Dey, 2016; Dey, 1999) have been developed as well (see., e.g., the review by Dey & Papanicolaou, 2008). Among these relationships, we used that of Cao et al. (2006). The critical shear stress for sediment erosion at the outer bank is $\tau_E = \tau_{*c}\,(\rho \Delta g d_s)$, with the critical Shields parameter τ_{*c} computed as

$$\begin{aligned} \tau_{*c} &= 0.1414\, R_p^{-0.23} && \left(R_p \le 6.61\right) \\ \tau_{*c} &= \frac{\left[1 + \left(0.0223\, R_p\right)^{2.84}\right]^{0.35}}{3.09\, R_p^{0.68}} && \left(6.61 < R_p \le 282.84\right) \\ \tau_{*c} &= 0.045 && \left(R_p \ge 282.84\right) \end{aligned} \tag{A1}$$

where $R_p = d\,(\Delta g d)^{0.5}\,/\nu$, with $\Delta = (\rho_s - \rho)/\rho$ the immersed relative density.

These relations are applicable for noncohesive material composing a river bank. Clearly, the presence of cohesive slump blocks can reduce the erosional power of the in-channel current (Parker et al., 2011). Slump blocks, in fact, shift the streamwise velocity away from the bank thus leading to a reduction of the shear stress acting on the bank toe. Even though it is possible to include explicitly this effect in the model, we propose to implicitly embed it in the PDF of channel width variations described in section 2.3.

The dimensionless critical shear stress for deposition is computed as

$$\tau_b = \frac{R_*^2}{\hat{d}^3}, \tag{A2}$$

where $R_* = u_*\, d/\nu$ is the shear Reynolds number, with $u_* = \tau/\rho$ the shear velocity, and $\hat{d}$ a dimensionless particle parameter that could be calculated as a function of either R_p or (Cheng, 1997)

$$\hat{d} = \sqrt{\frac{1}{1.2}\left(\frac{R_*\, w_s}{u_*}\right)^{2/3}\left[\left(\frac{R_*\, w_s}{u_*}\right)^{2/3} + 10\right]}. \tag{A3}$$

According to Bose and Dey (2013), the probability function P_s defining incipient suspension conditions is defined as

$$P_s = \frac{1}{16}\left[16 - \frac{u_*}{\sigma_w}\frac{w_s}{u_*} - \left(\frac{u_*}{\sigma_w}\frac{w_s}{u_*}\right)^2\right]\exp\left(-\frac{u_*}{\sigma_w}\frac{w_s}{u_*}\right), \tag{A4}$$

where σ_w is the root-mean-square of fluctuations of the instantaneous flow velocity in the vertical direction. This relation is used to obtain the value of w_s/u_* given the probability threshold for suspension, set as $P_s = 0.1$ in the present case, and recalling the relation proposed by Grass (1971)

$$\frac{\sigma_w}{u_*} = 1 - \exp\left(-0.093\, R_*^{1.3}\right) \tag{A5}$$

The value of w_s/u_* is then substituted in (A3), to obtain $\hat{d}$, and finally, τ_b is computed through (A2). It should be mentioned that the ratio u_*/w_s coincides with the mobility number Λ defined by Liu (1957), a parameter that can be used in alternative to the Shields number (Shields, 1936) for establishing the initiation of sediment motion.

Acknowledgments
The authors thank the AE, Patricia Saco, Kory Konsoer, and two other anonymous reviewers for the useful suggestions and inspiring comments that helped to improve the manuscript. The junior author wishes to thank the ERASMUS MUNDUS AMIDILA project that founded this research. The data used in the statistical elaborations and the source code for the model used in this study are available at https://zenodo.org/record/1467638\#.W83q-UvHxPY.

References

Abizaid, C. (2005). An anthropogenic meander cutoff along the Ucayali River, Peru. *American Geographical Society*, *95*(1), 122–135.
Ali, S. Z., & Dey, S. (2016). Hydrodynamics of sediment threshold. *Physics of Fluids*, *28*(7), 075103.

Asahi, K., Shimizu, Y., Nelson, J., & Parker, G. (2013). Numerical simulation of river meandering with self-evolving banks. *Journal of Geophysical Research: Earth Surface*, *118*, 2208–2229. https://doi.org/10.1002/jgrf.20150

Bartlett, M. S. (1937). Properties of sufficiency and statistical tests. *Proceedings of the Royal Society of London. Series A Mathematical and Physical Sciences*, *160*(901), 268–282.

Beheshti, A. A., & Ataie-Ashtiani, B. (2008). Analysis of threshold and incipient conditions for sediment movement. *Coastal Engineering*, *55*(5), 423–430.

Bhattacharyya, A. (1943). On a measure of divergence between two multinomial populations. *Sankhy?: The Indian Journal of Statistics (1933–1960)*, *7*(4), 401–406.

Blondeaux, P., & Seminara, G. (1985). A unified bar-bend theory of river meanders. *Journal of Fluid Mechanics*, *157*, 449–470.

Bogoni, M., Putti, M., & Lanzoni, S. (2017). Modeling meander morphodynamics over self-formed heterogeneous floodplains. *Water Resources Research*, *56*, 5137–5157. https://doi.org/10.1002/2017WR020726

Bolla Pittaluga, M., & Seminara, G. (2011). Nonlinearity and unsteadiness in river meandering: A review of progress in theory and modelling. *Earth Surface Processes and Landforms*, *36*(1), 20–38.

Bose, S. K., & Dey, S. (2013). Sediment entrainment probability and threshold of sediment suspension: An exponential based approach. *Journal of Hydraulic Engineering*, *139*(10), 1099–1106.

Brownlie, W. R. (1981). Prediction of flow depth and sediment discharge in open channels (*Technical Report No. KH-R-43A*). Pasadena, California: November, W. M. Keck Laboratory of Hydraulics and Water Resources, Division of Engineering and Applied Science, California Institute of Technology.

Camporeale, C., Perona, P., Porporato, A., & Ridolfi, L. (2005). On the long-term behavior of meandering rivers. *Water Resources Research*, *41*, W04109. https://doi.org/10.1029/2005WR004109

Camporeale, C., Perona, P., Porporato, A., & Ridolfi, L. (2007). Hierarchy of models for meandering rivers and related morphodynamic processes. *Reviews of Geophysics*, *45*, RG1001. https://doi.org/10.1029/2005RG000185

Cao, Z., Pender, G., & Meng, J. (2006). Explicit formulation of the Shields diagram for incipient. *Journal of Hydraulic Engineering*, *132*(10), 1097–1099.

Celik, I., & Rodi, W. W. (1991). Suspended sediment transport capacity for open channel flow. *Journal of Hydraulic Engineering*, *117*(2), 191–204.

Chen, D., & Duan, J. G. (2006). Modeling width adjustment in meandering channels. *Journal of Hydrology*, *321*, 59–76.

Cheng, N.-S. (1997). Simplified settling velocity formula for sediment particle. *Journal of Hydraulic Engineering*, *123*(2), 149–152.

Cheng, N.-S., & Chiew, Y.-M. (1999). Analysis of initiation of sediment suspension from bed load. *Journal of Hydraulic Engineering*, *125*(8), 855–861.

Constantine, J. A., Dunne, T., Ahmed, J., Legleiter, C., & Lazarus, E. D. (2014). Sediment supply as a driver of river meandering and floodplain evolution in the Amazon Basin. *Nature Geoscience*, *7*(12), 899–903.

Constantine, C. R., Dunne, T., & Hanson, G. J. (2009). Examining the physical meaning of the bank erosion coefficient used in meander migration modeling. *Geomorphology*, *106*(3-4), 242–252.

Darby, S. E., Alabyan, A. M., & Van de Wiel, M. J. (2002). Numerical simulation of bank erosion and channel migration in meandering rivers. *Water Resources Research*, *38*(9), W1163. https://doi.org/10.1029/2001WR000602

Darby, S. E., & Delbono, I. (2002). A model of equilibrium bed topography for meander bends with erodible banks. *Earth Surface Processes and Landforms*, *27*(10), 1057–1085.

Dey, S. (1999). Sediment threshold. *Applied Mathematical Modelling*, *23*(5), 399–417.

Dey, S., & Papanicolaou, A. (2008). Sediment threshold under stream flow: A state-of-the-art review. *Asce Journal of Civil Engineering*, *12*(1), 45–60.

Dryden, J. M., & Mardia, K. V. (2016). *Statistical shape analysis, with applications in R*. Chichester, UK: John Wiley.

Dunn, O. J. (1961). Multiple comparisons among means. *Journal of the American Statistical Association*, *56*(293), 52–64.

Eke, E. C., Czapiga, M. J., Viparelli, E., Shimizu, Y., Imran, J., Sun, T., & Parker, G. (2014). Coevolution of width and sinuosity in meandering rivers. *Journal of Fluid Mechanics*, *760*(5), 127–174.

Eke, E. C., Parker, G., & Shimizu, Y. (2014). Numerical modeling of erosional and depositional bank processes in migrating river bends with self-formed width: Morphodynamics of bar push and bank pull. *Journal of Geophysical Research: Earth Surface*, *119*, 1–29. https://doi.org/10.1002/2013JF003020

Ettmer, B., & Alvarado-Ancieta, C. A. (2010). Morphological development of the Ucayali River, Peru without human impacts. Basic results of topographical survey. *Waldökologie Landschaftsforschung und Naturschutz*, *10*, 77–84.

Frascati, A., & Lanzoni, S. (2009). Morphodynamic regime and long-term evolution of meandering rivers. *Journal of Geophysical Research*, *114*, F02002. https://doi.org/10.1029/2008JF001101

Frascati, A., & Lanzoni, S. (2010). Long-term river meandering as a part of chaotic dynamics? A contribution from mathematical modelling. *Earth Surface Processes and Landforms*, *35*(7), 791–802.

Frascati, A., & Lanzoni, S. (2013). A mathematical model for meandering rivers with varying width. *Journal of Geophysical Research: Earth Surface*, *118*, 1641–1657. https://doi.org/10.1002/jgrf.20084

Grass, A. J. (1971). Structural features of turbulent flow over smooth and rough boundaries. *Journal of Fluid Mechanics*, *50*(02), 233.

Güneralp, n., Abad, J. D., Zolezzi, G., & Hooke, J. M. (2012). Advances and challenges in meandering channels research. *Geomorphology*, *163–164*, 1–9.

H&O - ECSA (2005). Estudio de la navegabilidad del río Ucayali en el tramo comprendido entre Pucallpa y la confluencia con el río Marañón (*Technical report*): Dirección general de transporte acuático, Ministerio de transportes y comunicaciones.

Hooke, J. M. (2007). Complexity, self-organisation and variation in behaviour in meandering rivers. *Geomorphology*, *91*(3-4), 236–258.

Hooke, J. M. (2013). River meandering. In J. F. Shroder (Ed.), *Treatise on geomorphology* (pp. 260–288). San Diego, CA: Elsevier.

Howard, A. (1992). Modelling channel migration and floodplain sedimentation in meandering streams. In P. Carking & G. Petts (Eds.), *Lowland floodplain rivers* (pp. 1–41). Hoboken: John Wiley.

Howard, A. D., & Hemberger, A. T. (1991). Multivariate characterization of meandering. *Geomorphology*, *4*, 161–186.

Ikeda, S., Parker, G., & Sawai, K. (1981). Bend theory of river meanders. Part 1. Linear development. *Journal of Fluid Mechanics*, *112*, 363–377.

Kramer, H. (1935). Sand mixtures and sand movement in fluvial model. *Transactions of the American Society of Civil Engineers*, *100*(1), 798–838.

Kruskal, W. H., & Wallis, W. A. (1952). Use of ranks in one-criterion variance analysis. *Journal of the American Statistical Association*, *47*(260), 583–621.

Lanzoni, S., & Seminara, G. (2006). On the nature of meander instability. *Journal of Geophysical Research*, *111*, F04006. https://doi.org/10.1029/2005JF000416

Levene, H. (1960). Robust testes for equality of variances. In I. Olkin (Ed.), *Contributions to probability and statistics: Essays in honor of Harold Hotelling* (pp. 278–292). Palo Alto, CA: Stanford University Press.
Liu, H.-K. (1957). Mechanics of sediment ripple formation. *Journal of Hydraulic Division*, *83*(2), 1–23.
McFeeters, S. K. (1996). The use of normalized difference water index (NDWI) in the delineation of open water features. *International Journal of Remote Sensing*, *17*, 1425–1432.
Mehta, A. J., & Partheniades, E. (1975). An investigation of the depositional properties of flocculated fine sediments. *Journal of Hydraulic Research*, *134*, 22–1686.
Mood, A. M. (1954). On the asymptotic efficiency of certain nonparametric two-sample tests. *Annals of Mathematical Statistics*, *25*(3), 514–522.
Motta, D., Abad, J. D., Langendoen, E. J., & Garcia, M. H. (2012). A simplified 2D model for meander migration with physically-based bank evolution. *Geomorphology*, *163-164*, 10–25.
Nagata, N., Hosoda, T., & Muramoto, Y. (2000). Numerical analysis of river channel processes with bank erosion. *Journal of Hydraulic Engineering*, *126*(4), 243–252.
Parker, G., Seminara, G., & Solari, L. (2003). Bed load at low Shields stress on arbitrarily sloping beds: Alternative entrainment formulation. *Water Resources Research*, *39*(7), 1183. https://doi.org/10.1029/2001WR001253
Parker, G., Shimizu, Y., Wilkerson, G. V., Eke, E. C., Abad, J. D., Lauer, J. W., et al. (2011). A new framework for modeling the migration of meandering rivers. *Earth Surface Processes and Landforms*, *36*(1), 70–86.
SENAMHI (2016). Contenido: Comportamiento hidrológico de la cuenca amazónica durante el año hidrológico 2015-2016 (*Technical report*). Lima: Servicio Nacional de Meteorología e Hidrología del Perú - SENAMHI.
Santini, W., Martinez, J. M., Espinoza-Villar, R., Cochonneau, G., Vauchel, P., Moquet, J. S., et al. (2014). Sediment budget in the Ucayali River basin, an Andean tributary of the Amazon River. *IAHS-AISH Proceedings and Reports*, *367*(12), 320–325.
Scheffe, H. (1999). *The analysis of variance*. New York: Wiley-Interscience Publication.
Schwarz, G. (1978). Estimating the dimension of a model. *Annals of Statistics*, *6*(2), 461–464.
Schwenk, J., & Foufoula-Georgiou, E. (2016). Meander cutoffs nonlocally accelerate upstream and downstream migration and channel widening. *Geophysical Research Letters*, *43*, 12,437–12,445. https://doi.org/10.1002/2016GL071670
Schwenk, J., Khandelwal, A., Fratkin, M., Kumar, V., & Foufoula-Georgiou, E. (2017). High spatiotemporal resolution of river planform dynamics from Landsat: The RivMAP toolbox and results from the Ucayali River. *Earth and Space Science*, *4*, 46–75.
Schwenk, J., Lanzoni, S., & Foufoula-Georgiou, E. (2015). The life of a meander bend: Connecting shape and dynamics via analysis of a numerical model. *Journal of Geophysical Research: Earth Surface*, *120*, 690–710. https://doi.org/10.1002/2014JF003252
Seminara, G. (2006). Meanders. *Journal of Fluid Mechanics*, *554*, 271–297.
Shields, A. (1936). Application of similarity principles and turbulence research to bed-load movement. *Mitteilungen der Preussischen Versuchsanstalt fur Wasserbau und Schiffbau*, *26*, 5–24.
Simoes, F. J. M. (2014). Shear velocity criterion for incipient motion of sediment. *Water Science and Engineering*, *7*(2), 183–193.
Soulsby, R., & Whitehouse, R. (1997). Threshold of sediment motion in coastal environments. In N. Christchurch (Ed.), *Pacific coasts and ports '97: Proceedings of the 13th Australasian coastal and ocean engineering conference and the 6th Australasian port and harbour conference* (Vol. 1, pp. 149–154). University of Canterbury: Centre for Advanced Engineering.
Tukey, J. W. (1949). Comparing individual means in the analysis of variance. *Biometrics*, *5*(2), 99–114.
U.S. Geological Survey (2015). Landsat-Earth observation satellites (*Technical report*). Reston, VA: U.S. Geological Survey.
Van Rijn, L. C. (1984). Sediment transport. Part I: Bed load transport.
Wickert, A. D., Martin, J. M., Tal, M., Kim, W., Sheets, B., & Paola, C. (2013). River channel lateral mobility: Metrics, time scales, and controls. *Journal of Geophysical Research: Earth Surface*, *118*, 396–412. https://doi.org/10.1029/2012JF002386
Xu, H. (2006). Modification of normalised difference water index (NDWI) to enhance open water features in remotely sensed imagery. *International Journal of Remote Sensing*, *27*(14), 3025–3033.
Yalin, M. (1963). An expression for bed-load transportation. *Journal of Hydraulic Division*, *89*(3), 221–250.
Zolezzi, G., Luchi, R., & Tubino, M. (2012). Modeling morphodynamic processes in meandering rivers with spatial width variations. *Reviews of Geophysics*, *50*, RG4005. https://doi.org/10.1029/2012RG000392
Zolezzi, G., & Seminara, G. (2001). Downstream and upstream influence in river meandering. Part 1. General theory and application to over-deepening. *Journal of Fluid Mechanics*, *438*, 183–211.